1521-009X/42/8/1341–1348$25.00
Drug Metabolism and Disposition

http://dx.doi.org/10.1124/dmd.114.059188
Drug Metab Dispos 42:1341–1348, August 2014

Generation and Characterization of a Novel CYP2A13-Transgenic Mouse Model[S]

Kunzhi Jia, Lei Li, Zhihua Liu, Matthew Hartog, Kerri Kluetzman, Qing-Yu Zhang, and Xinxin Ding

Wadsworth Center, New York State Department of Health, and School of Public Health, State University of New York, Albany, New York

Received May 16, 2014; accepted June 3, 2014

ABSTRACT

***CYP2A13*, *CYP2B6*, and *CYP2F1* are neighboring cytochrome P450 genes on human chromosome 19, and the enzymes that they encode overlap in substrate specificity. A CYP2A13/2B6/2F1-transgenic mouse, in which CYP2A13 and 2F1 are both expressed in the respiratory tract and CYP2B6 is expressed in the liver, was recently generated. We generated a CYP2A13 (only) transgenic mouse so that the specific activity of CYP2A13 can be determined. The *CYP2B6* and *CYP2F1* genes in the *CYP2A13/2B6/2F1* genomic clone were inactivated via genetic manipulations, and *CYP2A13* was kept intact. A CYP2A13 (only) transgenic (2A13-TG) mouse was generated using the engineered construct and then characterized to confirm transgene integrity and determine copy numbers. The 2A13-TG mice were normal in gross morphology, development, and fertility. As in the CYP2A13/2B6/2F1-transgenic mouse, CYP2A13 expression in the 2A13-TG mouse was limited to the respiratory tract; in contrast, CYP2B6 and 2F1 proteins were not detected. Additional studies using the CYP2A13-humanized (2A13-TG/*Cyp2abfgs*-null) mouse produced by intercrossing between 2A13-TG and *Cyp2abfgs*-null mice confirmed that the transgenic CYP2A13 is active in the bioactivation of 4-(methylnitrosamino)-1-(3-pyridyl)-1-butanone (NNK), a lung procarcinogen. The 2A13-TG mouse should be valuable for assessing specific roles of human CYP2A13 in xenobiotic toxicity in the respiratory tract.**

Introduction

CYP2A13, a human cytochrome P450 enzyme preferentially expressed in the respiratory tract, is known through a number of in vitro studies to metabolize many xenobiotic compounds, including 4-(methylnitrosamino)-1-(3-pyridyl)-1-butanone (NNK) (Su et al., 2000), 4-aminobiphenyl (Nakajima et al., 2006), aflatoxin B_1 (He et al., 2006), naphthalene, styrene, and toluene (Fukami et al., 2008), and 3-methylindole (D'Agostino et al., 2009). For NNK, a tobacco-specific nitrosamine and potent lung carcinogen (Hecht, 2003), CYP2A13 is the most efficient enzyme in its metabolic activation (Su et al., 2000; Jalas et al., 2005). These findings led to the hypothesis that CYP2A13 plays an important role in the induction of lung tumorigenesis by NNK and possibly other tobacco carcinogens (Ding and Kaminsky, 2003; Megaraj et al., 2014). Consistent with this hypothesis, human light smokers who carry a variant *CYP2A13* allele (*2), which showed reduced expression as well as decreased enzyme activity toward NNK (D'Agostino et al., 2008), were found to be associated with a substantially reduced risk for lung adenocarcinoma (Wang et al., 2003). Nonetheless, definitive in vivo evidence for a role of CYP2A13 in tobacco-induced lung tumorigenesis has yet to be obtained.

Our recent study using a CYP2A13/2B6/2F1-transgenic mouse on a *Cyp2a5*-null background provided the first evidence that CYP2A13 and/or CYP2F1 is capable of mediating NNK-induced lung tumorigenesis in vivo (Megaraj et al., 2014). Compared with the *Cyp2a5*-null mouse, the CYP2A13/2B6/2F1-transgenic/*Cyp2a5*-null mouse showed significantly higher tumor incidence and frequency after NNK treatment. However, although the CYP2A13/2B6/2F1-transgenic mouse is valuable for determination of the collective functions of CYP2A13 and CYP2F1 in the lung (CYP2B6 is not expressed in the lung of the transgenic mouse), a CYP2A13 (only) transgenic (2A13-TG) mouse model would enable determination of the specific roles of CYP2A13 in vivo.

Here, we report the generation and characterization of a 2A13-TG mouse and its subsequent conversion to a CYP2A13-humanized mouse model on a novel *Cyp2abfgs*-null background. Given that the tissue specificity of the *CYP2A13* transgene expression in the original CYP2A13/2B6/2F1-transgenic mouse was similar to that in humans (Wei et al., 2012), we deduced that the 210-kilobase pair (kbp) human genomic DNA fragment that was used for generation of that mouse model contained all necessary regulatory sequences for tissue-specific CYP2A13 expression. Accordingly, we used the same *CYP2A13/2B6/2F1* genomic clone as starting material for preparation of the 2A13-TG construct via selective in vitro inactivation of the *CYP2B6* and *CYP2F1* genes.

NNK and most other known CYP2A13 substrates are also metabolized by one or more members of the mouse *Cyp2abfgs* gene subfamilies, many of which are also selectively expressed in the respiratory tract. Given the relatively low (but humanlike) expression level of the *CYP2A13* transgene in the transgenic mouse lung, the abundant expression of the mouse *Cyp2abfgs* genes will likely overshadow the

This work was supported in part by the National Institutes of Health National Cancer Institute [Grant CA092596 (to X.D.)] and National Institute of General Medical Sciences [Grant GM074249 (to Q.Z.)].

dx.doi.org/10.1124/dmd.114.059188.

[S] This article has supplemental material available at dmd.aspetjournals.org.

ABBREVIATIONS: 2A13-TG, CYP2A13 (only) transgenic; B6, C57BL/6; BAC, bacterial artificial chromosome; bp, base pair; FRT, flippase recognition target; HPB, 4-hydroxy-1-(3-pyridyl)-1-butanone; kbp, kilobase pair; NM, nasal mucosa; NNAL, 4-(methylnitrosamino)-1-(3-pyridyl)-1-butanol; NNK, 4-(methylnitrosamino)-1-(3-pyridyl)-1-butanone; Null, *Cyp2abfgs*-null; O^6-mG, O^6-methyl guanine; OPB, 4-oxo-4-(3-pyridyl)butanone; P450, cytochrome P450; PB, phenobarbital; TG, transgenic; WT, wild-type.

contributions of CYP2A13 to in vivo xenobiotic metabolism in the 2A13-TG mice, as shown recently for the CYP2A13/2B6/2F1-transgenic mouse (Wei et al., 2012). Previously, we used the *Cyp2a5*-null mouse to prepare a CYP2A13/2B6/2F1-humanized mouse (Megaraj et al., 2014), considering the orthologous relationship between CYP2A5 and CYP2A13. However, we have learned through recent studies using *Cyp2f2*-null, *Cyp2a(4/5)bgs*-null, and *Cyp2abfgs*-null mouse models that other members of the *Cyp2abfgs* gene cluster, particularly CYP2B and/or CYP2F2, are also quite active toward NNK and other CYP2A13 substrates, including naphthalene, 3-methylindole, and nicotine (Zhou et al., 2010, 2012a,b; Li et al., 2011, 2013; Megaraj et al., 2014). Therefore, to maximally reduce the background mouse lung P450 activity, we have prepared a 2A13-humanized mouse on the *Cyp2abfgs*-null background, in which all *Cyp2a, 2b, 2g, 2f*, and *2s* genes are deleted (Li et al., submitted manuscript). The 2A13-TG and/or 2A13-TG/*Cyp2abfgs*-null mice were characterized for viability, growth, and fertility; for the absence of CYP2B6 and CYP2F1 expression; for CYP2A13 transgene copy number and tissue distribution of *CYP2A13* transgene expression, both at the mRNA level and at the protein level; and for in vitro and in vivo activity toward NNK bioactivation.

Materials and Methods

Generation of the 2A13-TG Mouse Model. The human bacterial artificial chromosome (BAC) clone, ID number CTD-2535H15 (Invitrogen, Carlsbad, CA), containing *CYP2A13*, *CYP2B6*, and *CYP2F1* genes, which was used previously to generate the CYP2A13/2B6/2F1-TG model (Wei et al., 2012), was used as the starting material for preparation of the 2A13-TG transgene construct. The ~210-kbp BAC was modified to inactivate *CYP2F1* and *CYP2B6* with use of the counterselection BAC modification kit and Cre or FLP expression plasmid from Gene Bridges (Heidelberg, Germany). In brief, the engineering of the construct involved the following steps (Fig. 1).

Step 1. Generation of an *rpsL-neo* PCR product flanked by two 50-base pair (bp) homology arms targeting *CYP2F1* exon 10 at either side of the active-site cysteine (CYS) codon. The polymerase chain reaction (PCR) was performed using the *rpsL-neo* template provided in the counterselection BAC modification kit, the Platinum Pfx High-Fidelity DNA Polymerase (Invitrogen, Carlsbad, CA) and gel-purified primers

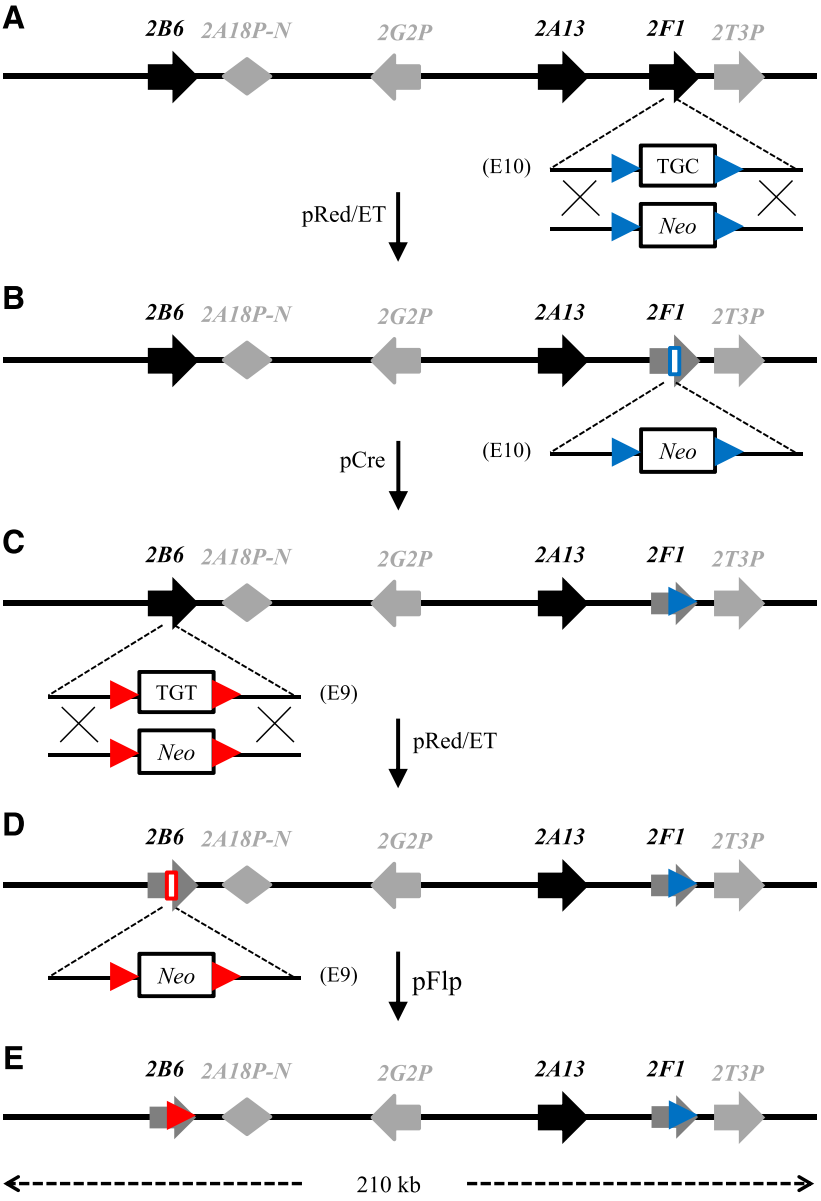

Fig. 1. Strategy for modification of the *CYP2A13/2B6/2F1* BAC clone to inactivate *CYP2F1* and *CYP2B6* and structure of the transgene. (A) Insertion of an rpsL-Neo cassette into *CYP2F1* exon 10 (E10) through Red/ET recombinase-mediated homologous recombination. The BAC clone contained *CYP2A13, CYP2B6,* and *CYP2F1* as well as three *CYP* pseudogenes (gray). The *Neo* gene is flanked by two 50-bp homology arms (each also containing one loxP site; blue arrowhead) that border the active site CYS codon (TGC) in the intact *CYP2F1* gene. (B) Removal of the rpsL-Neo cassette from the modified *CYP2F1* E10 via Cre-mediated recombination of the floxed sequence. (C) Insertion of an rpsL-neo cassette into *CYP2B6* exon 9 (E9) through Red/ET recombinase-mediated homologous recombination. The *Neo* gene is flanked by two 50-bp homology arms (each also containing one FRT site; red arrowhead) that border the active site CYS codon (TGT) in the intact *CYP2B6* gene. (D) Removal of the rpsL-neo cassette from the modified *CYP2B6* E9 via Flp-mediated recombination of the FRT-flanked sequence. (E) Final, linearized transgene construct with *CYP2F1* and *CYP2B6* inactivated.

2F1mE10F and 2F1mE10R (Supplemental Table 1) at an annealing temperature of 68°C. The resulting PCR product was composed of the CYP2F1 homology arms, a XhoI restriction enzyme site, and the *rpsL-neo* gene flanked by two loxP sites.

Step 2. Insertion of the floxed *rpsL-neo* cassette into the wild-type BAC through homologous recombination, with use of the Red/ET recombinase. Positive clones were identified through antibiotic selection.

Step 3. Removal of the *rpsl-neo* cassette through Cre-mediated recombination.

Step 4. DNA sequencing was used to confirm the modification of *CYP2F1* exon 10.

The process was then repeated for modification of the *CYP2B6* gene, using the BAC clone that contained the mutant *CYP2F1* as the starting material. For step 1, primers 2B61mE9F and 2B6mE9R (Supplemental Table 1) were used at an annealing temperature of 68°C, and the resulting PCR product was composed of the CYP2B6 homology arms, two stop codons, the *rpsL-neo* gene flanked by two flippase recognition target (FRT) sites, and a PspXI/XhoI site. In step 3, Flp recombinase was used to remove the FRT-flanked *rpsL-neo* cassette.

The ~210-kbp, modified BAC transgene construct (Fig. 1E) was linearized with Not I-HF (NEB, Ipswich, MA), which removes the vector, and isolated after pulsed-field gel electrophoresis and β-agarase (NEB) digestion, according to a published method (Abe et al., 2004). Transgenic mice were produced at the Transgenic and Knockout Core Facility at the Wadsworth Center, as described for the production of the CYP2A13/2B6/2F1-TG model (Wei et al., 2012). Purified BAC insert was microinjected into the pronuclei of fertilized eggs from the C57BL/6 (B6) strain. Positive transgenic mice were identified through PCR analysis of tail DNA for the detection of *CYP2A13* exon 5 (Wei et al., 2012).

The 2A13-TG mice were crossbred with *Cyp2abfgs*-null (Null) mice (Li et al., submitted manuscript), in which all mouse *Cyp2abfgs* genes are deleted; the resultant 2A13-TG$^{(+/-)}$/Null mice were used for detection of CYP2A13 mRNA expression, protein expression and activity, by comparing to the Null mice. Similarly, the CYP2A13/2B6/2F1-TG mice were also crossbred with the Null mice; the resultant CYP2A13/2B6/2F1-TG$^{(+/-)}$/Null mice were used as positive control for comparisons with 2A13-TG$^{(+/-)}$/Null. The same types of samples were also used for detection of CYP2F1 and CYP2B6 mRNA and protein expression. All studies with mice were approved by the Wadsworth Center Institutional Animal Care and Use Committee.

Southern Blot and Genomic DNA Sequence Analysis. Mouse genomic DNA was isolated from the thymus. Hind III-digested genomic DNA was fractionated by electrophoresis on 0.7% agarose gels, transferred to nylon membranes, and analyzed using a ^{32}P-labeled DNA probe corresponding to *CYP2A13* exon 2, as described elsewhere (Wei et al., 2012). The transgene copy number in 2A13-TG$^{(+/-)}$ mice was estimated through densitometric analysis of the 5.1-kbp *CYP2A13*-specific band detected, with DNA from CYP2A13/2B6/2F1-TG$^{(+/+)}$ mice as the positive control (and standard for quantification) and DNA from B6 wild-type (WT) mice as the negative control. Various amounts of genomic DNA from WT mice were added to CYP2A13/2B6/2F1-TG$^{(+/+)}$ genomic DNA (1–5 μg), to maintain a constant amount of total DNA (10 μg) for all samples analyzed. The 1-kb-plus DNA ladder (Invitrogen, Carlsbad, CA) was used for size determination.

Genomic DNA sequence at the sites of mutagenesis was determined from PCR products amplified using primers as shown (Supplemental Table 2), with genomic DNA isolated from mouse tail as the template. Restriction enzyme analysis of PCR products containing the CYP2B6 exon-9 region was performed by incubating 2 μg DNA with 100 U XhoI (NEB) overnight.

RNA-PCR Analysis. Total RNA was isolated using Trizol (Invitrogen). RNA samples were treated with DNase I (Invitrogen) before reverse transcription. For detection of CYP2F1 and CYP2B6 mRNAs, RNA-PCR was performed using a protocol described previously (Zhang et al., 2005; Wei et al., 2012), with use of gene-specific primers as described (Supplemental Table 2), and with primers for CYP2A13 mRNA as a positive control. For quantitative analysis of CYP2A13 expression, real-time RNA PCR was performed essentially as described previously elsewhere (Zhang et al., 2007) with primers specific for CYP2A13 (Zhang et al., 2004) and with glyceraldehyde 3-phosphate dehydrogenase (GAPDH) as a control (Wei et al., 2012). Serial dilutions of one reverse-transcription product were used to generate a standard curve.

Immunoblot Analysis. Microsomal proteins were prepared from various tissues of 2-month-old female mice, as described previously elsewhere (Ding and Coon, 1990). A rabbit anti-CYP2A5 polyclonal antibody (Gu et al., 1998) was used for detection of CYP2A13. Heterologously expressed CYP2A13 in a Sf9 cell microsomal preparation (Su et al., 2000) was used as the standard for CYP2A13 protein detection. A CYP2B6-specific monoclonal antibody (BD Gentest, Woburn, MA) was used for detection of CYP2B6 protein. A rabbit anti-CYP2F1/2 antibody (Li et al., 2011; Wei, et al., 2012) was used for detection of CYP2F1 protein. A recombinant CYP2F1, contained in a Sf9 cell microsomal preparation, was used as a positive control for immunoblot analysis (Wei et al., 2012). For immunoblot analysis, NuPAGE Bis-Tris mini-gels (10%) (Invitrogen) were used. Calnexin, a marker protein for the endoplasmic reticulum, was detected using a rabbit anti-human calnexin antibody (GenScript USA, Piscataway, NJ) and quantified as a loading control. Prestained protein markers (Precision-Plus, dual color; Bio-Rad Laboratories, Hercules, CA) were used for size estimation.

For detection of CYP2B6 in Null (negative control) and TG mice, 3- to 4-month-old female and male mice were treated once daily with phenobarbital (PB) at 80 mg/kg/d (i.p.) for 3 days. Mice were sacrificed 24 hours after the third injection, and livers from two mice per group were pooled for microsome preparation.

Assay for NNK Metabolism. The in vitro assay for NNK metabolism was performed as described previously elsewhere (Zhou et al., 2012a) with the use of 10 μM or 50 μM NNK, 5 mM sodium bisulfite, and 0.8 mg/ml (lung) or 0.1 mg/ml (nasal mucosa [NM]) microsomal protein. The initial rates of formation of 4-oxo-4-(3-pyridyl)butanone (OPB) and 4-hydroxy-1-(3-pyridyl)-1-butanone (HPB) were determined.

Determination of O^6-Methyl Guanine and Total Guanine in Mouse Genomic DNA. Mice were treated with a single i.p. injection of NNK (Chemsyn Science Laboratories, Lenexa, KS; dissolved in saline) at 100 mg/kg and were sacrificed 4 hours later. The lungs and livers were obtained for isolation of genomic DNA. O^6-methyl guanine (O^6-mG) levels and total guanine were determined with a liquid chromatography coupled with tandem mass spectrometry (LC-MS/MS) method and with a high-pressure liquid chromatography (HPLC) method, respectively, as described previously elsewhere (Weng et al., 2007).

Systemic NNK and NNAL Clearance. Mice were given a single i.p. injection (at 9:00–10:00 AM) of NNK at 100 mg/kg (in saline). For the preparation of plasma, blood samples (~20 μl each) were collected from the tail of individual mice at various time points (10 minutes to 4 hours) after the NNK injection. Plasma samples were processed for liquid chromatography/mass spectrometry analysis of NNK and 4-(methylnitrosamino)-1-(3-pyridyl)-1-butanol (NNAL), as described previously elsewhere (Weng et al., 2007; Zhou et al., 2010).

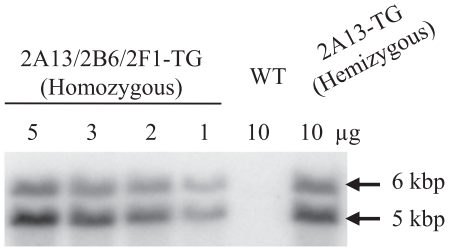

Fig. 2. Southern blot analysis of the transgene in 2A13-TG mice. An 864-bp CYP2A13 DNA probe (corresponding to parts of exon 2 and intron 2) was used. Genomic DNA was digested with Hind III. The size of the expected fragment from the *CYP2A13* transgene was 5.1 kb (from 5′-flanking region to exon 4). Genomic DNA from hemizygous 2A13-TG mice (10 μg) was compared with increasing amounts (1–5 μg) of genomic DNA from homozygous CYP2A13/2B6/2F1-TG mice (as positive control, five copies/genome), with genomic DNA from WT C57BL/6 mice (10 μg) as a negative control. To maintain equal abundance (10 μg) of total DNA in each lane, various amounts of genomic DNA from WT mice were also added to the positive control samples. Arrows represent the positions of selected bands in the 1-kb plus DNA ladder (Invitrogen). Densitometry analysis (not shown) of blots from two separate experiments indicated that the transgene copy number was ~3/genome in the 2A13-TG mice.

Results

Generation of the Transgenic Mouse Model. We modified the CYP2A13/2B6/2F1 BAC clone to inactivate the *CYP2F1* and *CYP2B6* genes while maintaining the function and regulation of the *CYP2A13* gene intact in the BAC clone. The genetic manipulations, as outlined in Fig. 1, would result in replacement of the critical active site CYS residue for both CYP2B6 and CYP2F1 by a small piece of exogenous DNA, which would further lead to either early termination of translation (for CYP2B6) or changes in the open reading frame for the remainder of the coding region (for CYP2F1), culminating in the absence of any WT CYP2B6 and CYP2F1 protein. The modified transgene would also retain sufficient amounts of 5′- and 3′-flanking sequences for insulation against potential integration-site effects on the *CYP2A13* transgene expression, as in the original *CYP2A13/2B6/2F*1 transgene (Wei et al., 2012).

A transgenic founder line (#3550) was identified through PCR-based detection of the *CYP2A13* exon 5 (data not shown). The founder was crossbred with B6 mice, and F1 pups were intercrossed to obtain homozygotes. Subsequent characterization of both hemizygotes and homozygotes indicated that the transgenic mice from line #3550 (hereafter named 2A13-TG) are normal in terms of gross morphology, development, and fertility (data not shown).

We estimated the transgene copy number by Southern blot analysis, with a DNA probe complementary to *CYP2A13* exon 2 and intron 2 (Fig. 2). Thymus DNA from a homozygous CYP2A13/2B6/2F1-transgenic mouse, with a transgene copy number of ~5 per genome (Wei et al., 2012), was used as standard for quantitation. The expected ~5-kbp Hind III fragment was detected in DNA samples from both the 2A13-TG mice and CYP2A13/2B6/2F1-TG mice; densitometric analysis of the relative band intensities in the various samples indicated that the copy number of the transgene in 2A13-TG mice was ~3/genome. No band was detected in genomic DNA from a WT mouse, a result confirming the specificity of the DNA probe used. An additional ~6-kbp band, most likely a Hind-III

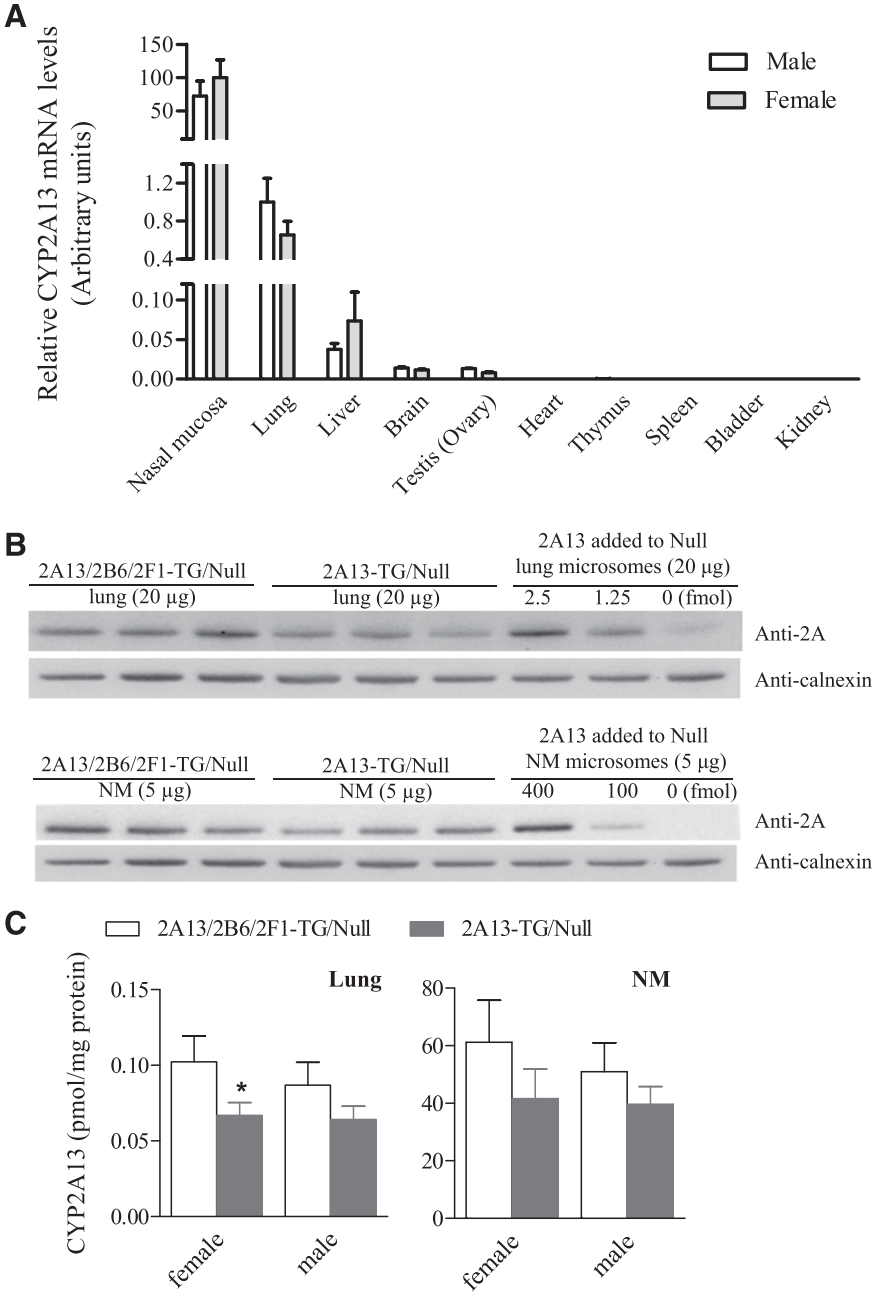

Fig. 3. Expression of the *CYP2A13* transgene. (A) Relative CYP2A13 mRNA expression levels in various tissues of hemizygous 2A13-TG/Null mice. Total RNA was isolated from tissues of 2-month-old male and female mice. The value presented (mean ± S.D., $n = 3$, in arbitrary units, relative to the male lung level) were normalized by the levels of mouse glyceraldehyde 3-phosphate dehydrogenase (GAPDH) transcript determined for the same samples. (B) Immunoblot detection of CYP2A13 protein in the lung and NM. Three different batches of lung (20 μg protein) and NM (5 μg protein) microsomal samples (each prepared from pooled tissues of five mice) from 2-month-old female Null, 2A13-TG/Null (hemizygous), and CYP2A13/2B6/2F1-TG/Null (hemizygous) mice ($n = 3$) were analyzed with use of an anti-CYP2A5 antibody. CYP2A13 standards (0–400 fmol, added to lung (20 μg) or NM (5 μg) microsomal protein from Null mice) were used for quantitative analysis. (C) Results of densitometric analysis of immunoblot data for both male and female mice ($n = 3$, mean ± S.D.). *$P < 0.05$. For either mouse strain, there was no significant sex difference in CYP2A13 protein levels.

fragment from *CYP2A18P-N* (included in the transgene construct), was also detected in 2A13-TG DNA samples, as it was in the CYP2A13/2B6/2F1-TG mice (Fig. 2) (Wei et al., 2012).

CYP2A13 Expression. CYP2A13 mRNA was detected by real-time PCR in several tissues of the 2A13-TG/Null mouse, including NM, lung, liver, brain, and testis (or ovary in female), but essentially not in bladder, heart, kidney, thymus, or spleen; the expression level in the NM was the highest, followed by the lung (Fig. 3A). This tissue expression profile was similar in male and female mice, and no sex difference in CYP2A13 mRNA levels was observed for any of the tissues examined.

The presence of abundant CYP2A5 protein in the lung interferes with the detection of transgenic CYP2A13 protein (Wei et al., 2012). However, CYP2A13 protein is readily detected in the lung and NM microsomes of 2A13-TG/Null mice as a result of the removal of all mouse *Cyp2abfgs* genes (Fig. 3B). In experiments not shown, CYP2A13 protein was not detected in the liver, brain, or testis. A densitometric analysis showed that the content of CYP2A13 protein in 2A13-TG$^{(+/-)}$/Null mouse lung and NM microsomes was ~70% of that in corresponding microsomal samples from CYP2A13/2B6/2F1-TG$^{(+/-)}$/Null mice.

Confirmation That CYP2B6 and CYP2F1 Are Not Expressed in 2A13-TG Mouse. Several approaches were taken to confirm that the *CYP2B6* and *CYP2F1* genes have been mutated as designed, and that these genes are no longer expressed. The structural changes at the CYP2B6 and CYP2F1 loci were confirmed by sequencing PCR products encompassing the mutated region, amplified from genomic DNA of hemizygous 2A13-TG/Null mice and, as a control, CYP2A13/2B6/2F1-TG/Null mice (Fig. 4A, and Fig. 5A). The genomic PCR products were also analyzed by agarose gel electrophoresis, either directly, to show size difference of the mutated region (for CYP2F1), or after restriction digest with XhoI, to show differing restriction profiles (for CYP2B6), between the two strains of TG mice (Fig. 4B, and Fig. 5B).

CYP2F1 mRNA was not detected in the lungs or NM of hemizygous 2A13-TG/Null mice when analyzed using PCR primers specific for the WT sequence; as a control, CYP2F1 was readily detected in these tissues from the CYP2A13/2B6/2F1-TG/Null mice (Fig. 4C). Similarly, CYP2B6 mRNA was detected in the liver and NM tissues of CYP2A13/2B6/2F1-TG/Null mice, but not in these tissues from hemizygous 2A13-TG/Null mice (Fig. 5C).

Expression of CYP2B6 and CYP2F1 protein was also analyzed in 2A13-TG/Null and CYP2A13/2B6/2F1-TG/Null (i.e., "humanized") mice, using Null mice as a negative control. The use of the humanized mice avoids interference by mouse CYP2F2 and CYP2B proteins. As shown in Fig. 4D, CYP2F1 protein was not detected in lung or NM microsomes from either 2A13-TG/Null or Null mice but was detected in lung and NM microsomes from CYP2A13/2B6/2F1-TG/Null mice.

For detection of CYP2B6 protein, PB-treated mice were analyzed to maximize the sensitivity of detecting CYP2B6 in the TG mice. The transgenic CYP2B6 has been found to be highly inducible by PB in the liver of the CYP2A13/2B6/2F1-TG mice (Liu et al., unpublished data). However, as shown in Fig. 5D, CYP2B6 protein was not detected in liver microsomes from either 2A13-TG/Null or Null mice, but was abundantly detected in liver microsomes from CYP2A13/2B6/2F1-TG/Null mice.

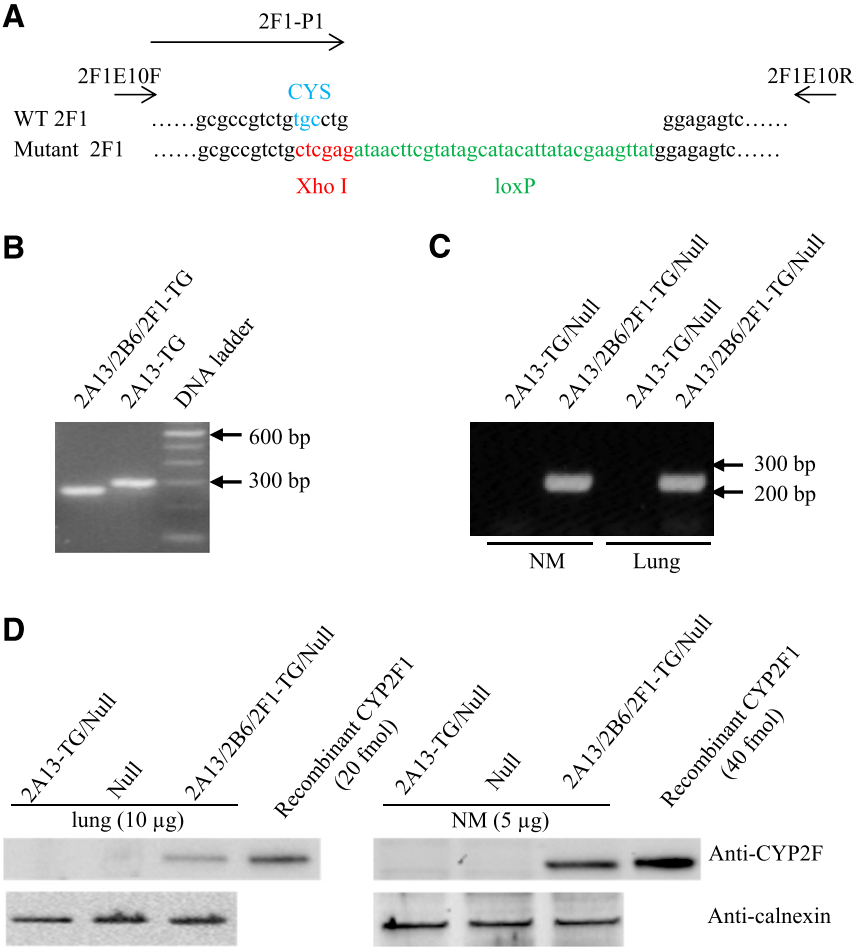

Fig. 4. Confirmation that CYP2F1 was inactivated and not expressed. (A) DNA sequence determined for WT and mutant CYP2F1 exon-10 region. The CYS codon (blue) and three additional nucleotides in WT CYP2F1 was replaced by an XhoI restriction site (red) and a loxP sequence (green), making the mutant E10 34 bp longer than WT E10. The sequence was determined (using primer 2F1E10F) from PCR products amplified (using primers 2F1E10F and 2F1E10R; Supplemental Table 2) from genomic DNA of a hemizygous 2A13-TG (mutant CYP2F1) or CYP2A13/2B6/2F1-TG (WT CYP2F1) female mouse. The approximate positions of PCR primers are also indicated. (B) PCR products used for sequence analysis in A; the product from 2A13-TG was larger. Arrows represent the positions of selected bands in the 100 bp DNA ladder (Invitrogen). (C) RNA-PCR detection of WT CYP2F1. RNA was prepared from the NM and lungs of adult female hemizygous 2A13-TG/Null or CYP2A13/2B6/2F1-TG/Null mice (pooled from two mice per sample). PCR was performed using primers 2F1-P1 (specific for WT 2F1) and 2F1E10R (Supplemental Table 2). The PCR product (222 bp) was analyzed on an agarose gel and visualized by staining with ethidium bromide. CYP2A13 was analyzed as the positive control (not shown). Arrows represent the positions of selected bands in the 100-bp DNA ladder (Invitrogen). Typical results are shown. (D) Immunoblot detection of CYP2F1 protein. Lung and NM microsomes from adult female Null, 2A13-TG/Null, and CYP2A13/2B6/2F1-TG/Null mice [10 μg (lung) or 5 μg (NM) protein per lane; pooled tissues from two to five mice per sample] were analyzed using an anti-CYP2F antibody or an anti-calnexin antibody. A recombinant CYP2F1 standard (20–40 fmol) was also analyzed as a positive control. Typical results are shown. Similar results were found in male mice (data not shown).

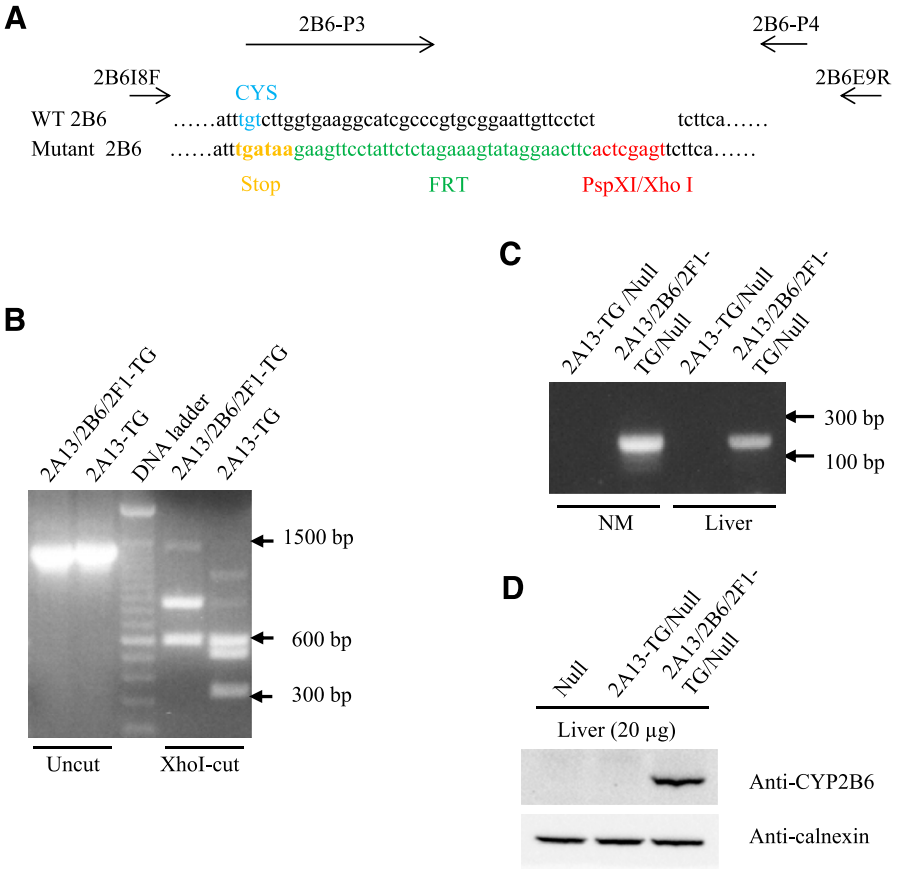

Fig. 5. Confirmation that CYP2B6 was inactivated and not expressed. (A) DNA sequence determined for WT and mutant CYP2B6 exon-9 region. The CYS codon (blue) and 37 additional nucleotides in WT CYP2B6 were replaced by, sequentially, two stop codons (orange), a FRT sequence (green), and a PspXI/XhoI restriction site (red). The sequence was determined (using primer 2B6E9R) from PCR products (1.4 kbp) amplified (using primers 2B6I8F and 2B6E9R; Supplemental Table 2) from the genomic DNA of a hemizygous 2A13-TG (mutant CYP2B6) or CYP2A13/2B6/2F1-TG (WT CYP2B6) female mouse. The approximate positions of PCR primers are also indicated. (B) Restriction enzyme analysis of PCR products containing the CYP2B6 exon-9 region. The PCR products were either uncut or treated with XhoI. The profile of restriction fragments is consistent with the presence of an additional XhoI site in the PCR product from 2A13-TG, compared with CYP2A13/2B6/2F1-TG. Arrows represent the positions of selected bands in the 100-bp DNA ladder (Invitrogen). (C) RNA-PCR detection of WT CYP2B6. RNA was prepared from NM and liver of adult female hemizygous 2A13-TG/Null or CYP2A13/2B6/2F1-TG/Null mice (pooled tissues from two mice per sample). PCR was performed using primers 2B6-P3 (specific for WT 2B6) and 2B6-P4 (Supplemental Table 2). The PCR product (171 bp) was analyzed on an agarose gel and visualized by staining with ethidium bromide. CYP2A13 was also analyzed as positive control (not shown). Arrows represent the positions of selected bands in the 1-kb-plus DNA ladder (Invitrogen). Typical results are shown. (D) Immunoblot detection of CYP2B6 protein. Liver microsomes from adult female Null, 2A13-TG/Null, and CYP2A13/2B6/2F1-TG/Null mice (20 μg protein per lane; from tissues pooled from two mice) were analyzed using an anti-CYP2B6 monoclonal antibody. Calnexin was analyzed as a loading control. Mice were pretreated with PB to induce CYP2B6 expression, as described in *Materials and Methods*. Similar results were obtained in male mice (data not shown).

NNK Bioactivation in Lung and NM of 2A13-TG Mice. Microsomes prepared from lung and NM of Null and 2A13-TG/Null mice were analyzed for in vitro metabolic activities toward NNK, a CYP2A13 substrate. Formation rates of two stable metabolites (OPB and HPB) of NNK were determined at two different NNK concentrations (10 and 50 μM). As shown in Table 1, the formation rates of OPB, representing the α-hydroxylation pathway that leads to O^6-mG DNA adduct formation (Peterson et al., 1993; Hecht, 1998), were ~2-fold (lung) and ~7- to 12-fold (NM) higher in microsomes from 2A13-TG/Null mice compared with Null mice. The formation rates of the HPB, representing the α-hydroxylation pathway that leads to NNK-DNA adduct formation, which enhances the persistence of O^6-mG by inhibiting DNA repair (Peterson et al., 1993; Liu et al., 1996), were also higher by ~2-fold (lung) and ~67–70 fold (NM) in microsomes from 2A13-TG/Null mice relative to Null.

In vivo formation of O^6-mG was also examined in NNK-treated Null and 2A13-TG/Null mice at a NNK dose used for lung tumor bioassays (100 mg/kg) (Weng et al., 2007). The abundance of hepatic O^6-mG was similar between the two mouse strains (Table 2), consistent with the negligible expression and function of CYP2A13 in the liver. In the

TABLE 1

NNK metabolic activation by lung and NM microsomes

Microsomal NNK metabolism was assayed as described under Materials and Methods. Rates of OPB and HPB formation (mean ± S.D., n = 3) were determined, with NNK at 10 μM or 50 μM. Microsomal samples were prepared from pooled tissues of two (lung) to four (NM) 2-month-old female *Cyp2abfgs*-null (Null) and 2A13-TG/Null mice.

Tissue	Strain	NNK Concentration	Rates of Product Formation	
			OPB	HPB
		μM	*pmol/min/mg protein*	
Lung	Null	10	2.87 ± 0.40	16.6 ± 3.9
	2A13-TG/Null		4.96 ± 0.14[a]	24.5 ± 3.8
	Null	50	10.6 ± 0.4	17.7 ± 2.7
	2A13-TG/Null		22.7 ± 4.5[b]	41.4 ± 8.1[b]
Nasal mucosa	Null	10	2.13 ± 1.05	0.81 ± 0.41
	2A13-TG/Null		24.9 ± 8.5[b]	54.0 ± 11.3[b]
	Null	50	9.58 ± 1.58	1.63 ± 0.21
	2A13-TG/Null		64.3 ± 13.8[b]	115 ± 17[a]

[a] $P < 0.001$, compared with Null mice (Student's t test).
[b] $P < 0.01$, compared with Null mice (Student's t test).

TABLE 2

NNK-induced O^6-mG adduct formation in vivo

Null and 2A13-TG/Null (2-month-old female) mice were injected with NNK at a dose of 100 mg/kg (i.p.), and tissue levels of O^6-mG and total guanine were determined 4 hours after the injection. Data represent mean ± S.D. (n = 4).

Strain	O^6-mG Level	
	Lung	Liver
	pmol/μmol guanine	
Null	<1.0[a]	445 ± 100
2A13-TG/Null	9.7 ± 3.0	435 ± 40

[a]Below detection limit.

lungs, although O^6-mG level in the Null mice was below detection limit (~1 pmol/μmol guanine), it was detected at ~10 pmol/μmol guanine in the 2A13-TG/Null mice, representing a 10-fold or greater increase. In control experiments, we confirmed that systemic clearance of NNK and its main circulating metabolite NNAL was not different between the two strains of mice (Fig. 6, A and B). Collectively, these data indicate that the transgenic CYP2A13 is functional and further support our previous finding in the CYP2A13/2B6/2F1-TG mice that lung CYP2A13 contributes significantly to the target tissue metabolic activation of NNK, a potent lung procarcinogen.

Discussion

In this study, we have successfully accomplished the goal of achieving adequate, humanlike CYP2A13 expression in a mouse model without the coexpression of the neighboring *CYP2B6* and *CYP2F1* genes. Furthermore, we have confirmed that the transgenic CYP2A13 is functional in the bioactivation of NNK, thus validating the usefulness of the 2A13-TG model for in vivo functional studies on the specific role of CYP2A13 in xenobiotic toxicity in the respiratory tract. By comparing the 2A13-TG model and the CYP2A13/2B6/2F1-transgenic mouse model, we should be able to delineate the respective contributions of CYP2A13 and CYP2F1 to xenobiotic metabolism in the lung. In that regard, the 2A13-TG model and the CYP2A13/2B6/2F1 transgenic model have subtle differences in CYP2A13 expression levels (~35% lower in 2A13-TG), which most likely resulted from differences in *CYP2A13* transgene copy number (3 in 2A13-TG and 5 in CYP2A13/2B6/2F1-transgenic). This difference in CYP2A13 expression level should be corrected for when P450 activity is directly compared between the two mouse models. Additionally, only hemizygous 2A13-TG mice were studied here; it is expected that the CYP2A13 expression level and activity in homozygous 2A13-TG mice will be twice as high as in the hemizygotes.

The transgene construct was prepared by mutating the *CYP2B6* and *CYP2F1* genes in the *CYP2A13/2B6/2F1* transgene construct that was previously used to produce the CYP2A13/2B6/2F1-transgenic mouse model (Wei et al., 2012). This approach, which required genetic manipulation of the large BAC clone, made it possible to maximally preserve flanking genomic sequences that are potentially critical for tissue-specific expression of the *CYP2A13* transgene. In that regard, we had previously found it challenging to reproduce the endogenous gene expression profile in transgenic mice for rat *CYP2A3* (the ortholog of human *CYP2A13*) when using a transgene construct that contained only 3.4 kbp of the 5′-flanking sequence and 1.5-kbp 3′-flanking sequence (Su et al., 2002). The humanlike tissue-selective expression of CYP2A13 in two independent mouse models, the original CYP2A13/2B6/2F1-transgenic mouse model (Wei et al., 2012) and the present 2A13-TG model, strongly supports the notion that the regulatory sequence for tissue-specific CYP2A13 expression is contained in the BAC transgene fragment that was used for production of the mouse models.

Human CYP-transgenic mouse models are often produced using source DNA contained in BAC clones, which typically contain multiple genes (Zhang et al., 2012). The successful generation of the 2A13-TG model through BAC mutagenesis illustrates effectiveness of this strategy for generating transgenic mice that selectively express one or more, but not all, genes in a cluster of closely linked genes. In that regard, several human P450 gene clusters exist, including *CYP1A*, *CYP2ABFGST* (where *CYP2A13* is located), *CYP2C*, *CYP3A*, *CYP4ABXZ*, and *CYP4F* (Nelson et al., 2004). In addition to the CYP2A13/2B6/2F1-transgenic mouse (Wei et al., 2012), a CYP2C18/19 transgenic mouse (Löfgren et al., 2009) and a CYP1A1/2 transgenic mouse (Jiang et al., 2005) have also been reported, where more than one human *CYP* genes coexpress in the mouse model. Application of our approach will possibly allow production of single-gene transgenic models for these gene clusters as well.

This is one of the first studies that illustrate the utility of the *Cyp2abfgs*-null model for production of a CYP-humanized mouse. The level of transgenic CYP2A13 in lung microsomes of the hemizygous 2A13-TG mouse (~70 fmol/mg protein), although still somewhat higher than the CYP2A13 levels found in microsomal preparations from human lung biopsy samples (≤20 fmol/mg protein; Zhang et al., 2007), is low compared with the levels of relevant mouse lung P450s such as CYP2A5 (~5 pmol/mg protein; Wei et al., 2012). Therefore, the 2A13-TG mouse was cross-bred with the *Cyp2abfgs*-null mouse to generate a "humanized" mouse model that expresses human CYP2A13 but not any of the mouse *Cyp2abfgs* genes. The advantage of studying CYP2A13 function on the *Cyp2abfgs*-null

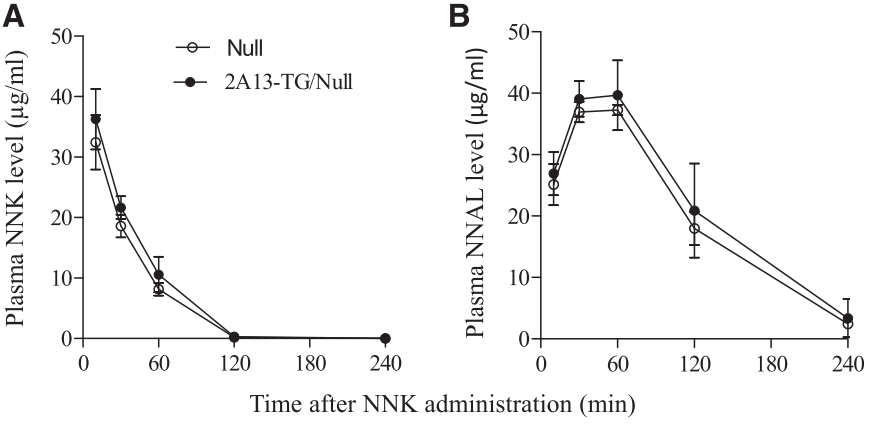

Fig. 6. Pharmacokinetics of NNK and NNAL. Plasma levels of NNK and NNAL were determined at various time points after administration of NNK (100 mg/kg, i.p.) to Null and 2A13-TG/Null mice (2-month-old, female). Data represent mean ± S.D. (n = 4).

background—compared with the *Cyp2a5*-null background—is clear when we compare the activity data from this study with data from the CYP2A13/2B6/2F1-transgenic/*Cyp2a5*-null model (Megaraj et al., 2014). For example, it was more convincing when demonstrating the role of CYP2A13 in NNK bioactivation in vivo in this study (9.7 ± 3.0 versus <1.0 pmol/μmol guanine in lung O^6-mG level) than in the earlier work (28.0 ± 2.0 versus 20.2 ± 1.6 pmol/μmol guanine in lung O^6-mG level). The difference between the *Cyp2a5*-null and *Cyp2abfgs*-null mice in NNK bioactivation has been reported elsewhere (Zhou et al., 2012a; Li et al., submitted manuscript), which indicated the role of other mouse *Cyp2abfgs* genes (besides *Cyp2a5*) in NNK metabolism/bioactivation and tumorigenesis.

To summarize, we have generated a novel transgenic mouse model in which human CYP2A13 but not the closed associated CYP2F1 or CYP2B6 is expressed preferentially in the NM and lung. The transgenic CYP2A13 is active toward the lung carcinogen NNK both in vitro and in vivo. The activity of the transgenic CYP2A13 can be readily demonstrated in a humanized 2A13-TG/*Cyp2abfgs*-null mouse; the latter will be valuable for studies on the role of CYP2A13 as a risk factor as well as therapeutic target for xenobiotic-induced lung toxicity and tumorigenesis.

Acknowledgments

The authors thankfully acknowledge the use of the services of the Biochemistry, Molecular Genetics, Pathology, and Transgenic and Knockout Mouse Core Facilities of the Wadsworth Center, New York State Department of Health. The authors also thank Drs. Bruce Herron and Yuan Wei for helpful discussion and assistance with BAC modification.

Authorship Contributions

Participated in research design: Jia, Li, Kluetzman, Zhang, Ding.
Conducted experiments: Jia, Li, Liu, Hartog, Kluetzman.
Performed data analysis: Jia, Li, Liu, Hartog, Zhang, Ding.
Wrote or contributed to the writing of the manuscript: Jia, Li, Zhang, Ding.

References

Abe K, Hazama M, Katoh H, Yamamura K, and Suzuki M (2004) Establishment of an efficient BAC transgenesis protocol and its application to functional characterization of the mouse Brachyury locus. *Exp Anim* **53**:311–320.

D'Agostino J, Zhang X, Wu H, Ling G, Wang S, Zhang QY, Liu F, and Ding X (2008) Characterization of CYP2A13*2, a variant cytochrome P450 allele previously found to be associated with decreased incidences of lung adenocarcinoma in smokers. *Drug Metab Dispos* **36**: 2316–2323.

D'Agostino J, Zhuo X, Shadid M, Morgan DG, Zhang X, Humphreys WG, Shu YZ, Yost GS, and Ding X (2009) The pneumotoxin 3-methylindole is a substrate and a mechanism-based inactivator of CYP2A13, a human cytochrome P450 enzyme preferentially expressed in the respiratory tract. *Drug Metab Dispos* **37**:2018–2027.

Ding X and Coon MJ (1990) Immunochemical characterization of multiple forms of cytochrome P-450 in rabbit nasal microsomes and evidence for tissue-specific expression of P-450s NMa and NMb. *Mol Pharmacol* **37**:489–496.

Ding X and Kaminsky LS (2003) Human extrahepatic cytochromes P450: function in xenobiotic metabolism and tissue-selective chemical toxicity in the respiratory and gastrointestinal tracts. *Annu Rev Pharmacol Toxicol* **43**:149–173.

Fukami T, Katoh M, Yamazaki H, Yokoi T, and Nakajima M (2008) Human cytochrome P450 2A13 efficiently metabolizes chemicals in air pollutants: naphthalene, styrene, and toluene. *Chem Res Toxicol* **21**:720–725.

Gu J, Zhang QY, Genter MB, Lipinskas TW, Negishi M, Nebert DW, and Ding X (1998) Purification and characterization of heterologously expressed mouse CYP2A5 and CYP2G1: role in metabolic activation of acetaminophen and 2,6-dichlorobenzonitrile in mouse olfactory mucosal microsomes. *J Pharmacol Exp Ther* **285**:1287–1295.

He XY, Tang L, Wang SL, Cai QS, Wang JS, and Hong JY (2006) Efficient activation of aflatoxin B1 by cytochrome P450 2A13, an enzyme predominantly expressed in human respiratory tract. *Int J Cancer* **118**:2665–2671.

Hecht SS (1998) Biochemistry, biology, and carcinogenicity of tobacco-specific N-nitrosamines. *Chem Res Toxicol* **11**:559–603.

Hecht SS (2003) Tobacco carcinogens, their biomarkers and tobacco-induced cancer. *Nat Rev Cancer* **3**:733–744.

Jalas JR, Hecht SS, and Murphy SE (2005) Cytochrome P450 enzymes as catalysts of metabolism of 4-(methylnitrosamino)-1-(3-pyridyl)-1-butanone, a tobacco specific carcinogen. *Chem Res Toxicol* **18**:95–110.

Jiang Z, Dalton TP, Jin L, Wang B, Tsuneoka Y, Shertzer HG, Deka R, and Nebert DW (2005) Toward the evaluation of function in genetic variability: characterizing human SNP frequencies and establishing BAC-transgenic mice carrying the human *CYP1A1_CYP1A2* locus. *Hum Mutat* **25**:196–206.

Li L, Jia K, Zhou X, McCallum SE, Hough LB, and Ding X (2013) Impact of nicotine metabolism on nicotine's pharmacological effects and behavioral responses: insights from a Cyp2a(4/5)bgs-null mouse. *J Pharmacol Exp Ther* **347**:746–754.

Li L, Wei Y, Van Winkle L, Zhang QY, Zhou X, Hu J, Xie F, Kluetzman K, and Ding X (2011) Generation and characterization of a *Cyp2f2*-null mouse and studies on the role of CYP2F2 in naphthalene-induced toxicity in the lung and nasal olfactory mucosa. *J Pharmacol Exp Ther* **339**:62–71.

Liu XK, Spratt TE, Murphy SE, and Peterson LA (1996) Pyridyloxobutylation of guanine residues by 4-[(acetoxymethyl)nitrosamino]-1-(3-pyridyl)-1-butanone generates substrates of O6-alkylguanine-DNA alkyltransferase. *Chem Res Toxicol* **9**:949–953.

Löfgren S, Baldwin RM, Carlerös M, Terelius Y, Fransson-Steen R, Mwinyi J, Waxman DJ, and Ingelman-Sundberg M (2009) Regulation of human CYP2C18 and CYP2C19 in transgenic mice: influence of castration, testosterone, and growth hormone. *Drug Metab Dispos* **37**:1505–1512.

Megaraj V, Zhou X, Xie F, Liu Z, Yang W, and Ding X (2014) Role of CYP2A13 in the bioactivation and lung tumorigenicity of the tobacco-specific lung procarcinogen 4-(methylnitrosamino)-1-(3-pyridyl)-1-butanone: *in vivo* studies using a CYP2A13-humanized mouse model. *Carcinogenesis* **35**: 131–137.

Nakajima M, Itoh M, Sakai H, Fukami T, Katoh M, Yamazaki H, Kadlubar FF, Imaoka S, Funae Y, and Yokoi T (2006) CYP2A13 expressed in human bladder metabolically activates 4-aminobiphenyl. *Int J Cancer* **119**:2520–2526.

Nelson DR, Zeldin DC, Hoffman SM, Maltais LJ, Wain HM, and Nebert DW (2004) Comparison of cytochrome P450 (CYP) genes from the mouse and human genomes, including nomenclature recommendations for genes, pseudogenes and alternative-splice variants. *Pharmacogenetics* **14**:1–18.

Peterson LA, Liu XK, and Hecht SS (1993) Pyridyloxobutyl DNA adducts inhibit the repair of O6-methylguanine. *Cancer Res* **53**:2780–2785.

Su T, Bao Z, Zhang QY, Smith TJ, Hong JY, and Ding X (2000) Human cytochrome P450 CYP2A13: predominant expression in the respiratory tract and its high efficiency metabolic activation of a tobacco-specific carcinogen, 4-(methylnitrosamino)-1-(3-pyridyl)-1-butanone. *Cancer Res* **60**:5074–5079.

Su T, Zhang QY, Zhang J, Swiatek P, and Ding X (2002) Expression of the rat CYP2A3 gene in transgenic mice. *Drug Metab Dispos* **30**:548–552.

Wang H, Donley KM, Keeney DS, and Hoffman SM (2003) Organization and evolution of the *Cyp2* gene cluster on mouse chromosome 7, and comparison with the syntenic human cluster. *Environ Health Perspect* **111**:1835–1842.

Wei Y, Wu H, Li L, Liu Z, Zhou X, Zhang QY, Weng Y, D'Agostino J, Ling G, and Zhang X, et al. (2012) Generation and characterization of a CYP2A13/2B6/2F1-transgenic mouse model. *Drug Metab Dispos* **40**:1144–1150.

Weng Y, Fang C, Turesky RJ, Behr M, Kaminsky LS, and Ding X (2007) Determination of the role of target tissue metabolism in lung carcinogenesis using conditional cytochrome P450 reductase-null mice. *Cancer Res* **67**:7825–7832.

Zhang D, Luo G, Ding X, and Lu C (2012) Preclinical experimental models of drug metabolism and disposition in drug discovery and development. *Acta Pharm Sin B* **2**:549–561 DOI: 10.1016/j.apsb.2012.10.004.

Zhang X, Caggana M, Cutler TL, and Ding X (2004) Development of a real-time polymerase chain reaction-based method for the measurement of relative allelic expression and identification of CYP2A13 alleles with decreased expression in human lung. *J Pharmacol Exp Ther* **311**:373–381.

Zhang X, D'Agostino J, Wu H, Zhang QY, von Weymarn L, Murphy SE, and Ding X (2007) CYP2A13: variable expression and role in human lung microsomal metabolic activation of the tobacco-specific carcinogen 4-(methylnitrosamino)-1-(3-pyridyl)-1-butanone. *J Pharmacol Exp Ther* **323**:570–578.

Zhang X, Zhang Q-Y, Liu D, Su T, Weng Y, Ling G, Chen Y, Gu J, Schilling B, and Ding X (2005) Expression of cytochrome p450 and other biotransformation genes in fetal and adult human nasal mucosa. *Drug Metab Dispos* **33**:1423–1428.

Zhou X, D'Agostino J, Li L, Moore CD, Yost GS, and Ding X (2012a) Respective roles of CYP2A5 and CYP2F2 in the bioactivation of 3-methylindole in mouse olfactory mucosa and lung: studies using *Cyp2a5*-null and *Cyp2f2*-null mouse models. *Drug Metab Dispos* **40**:642–647.

Zhou X, D'Agostino J, Xie F, and Ding X (2012b) Role of CYP2A5 in the bioactivation of the lung carcinogen 4-(methylnitrosamino)-1-(3-pyridyl)-1-butanone in mice. *J Pharmacol Exp Ther* **341**:233–241.

Zhou X, Zhuo X, Xie F, Kluetzman K, Shu YZ, Humphreys WG, and Ding X (2010) Role of CYP2A5 in the clearance of nicotine and cotinine: insights from studies on a *Cyp2a5*-null mouse model. *J Pharmacol Exp Ther* **332**:578–587.

Address correspondence to: Dr. Xinxin Ding, SUNY College of Nanoscale Science and Engineering, 257 Fuller Road, Albany, NY 12203. E-mail: xding@albany.edu